Hydrographic changes in the eastern subpolar North Atlantic during the last deglaciation

Heather M. Benway[a], Jerry F. McManus[b], Delia W. Oppo[c], James L. Cullen[d]

[a] *Department of Marine Chemistry & Geochemistry, MS #25, Woods Hole Oceanographic Institution, Woods Hole, MA, 02543, USA*

[b] *Lamont-Doherty Earth Observatory, 61 Route 9W - PO Box 1000 Palisades, NY 10964-8000, USA*

[c] *Department of Geology & Geophysics, MS #23, Woods Hole Oceanographic Institution, Woods Hole, MA, 02543, USA*

[d] *Department of Geological Sciences, Salem State College, Salem, MA 01970, USA*

Corresponding Author:
Heather Benway
Department of Marine Chemistry and Geochemistry
Woods Hole Oceanographic Institution
Mailstop #25
Woods Hole, MA 02543 USA
Phone: (508) 289-2838
Fax: (508) 457-2193 (fax)
Email: hbenway@whoi.edu

Abstract:
Millennial-scale climate fluctuations of the last deglaciation have been tied to abrupt changes in the Atlantic Meridional Overturning Circulation (MOC). A key to understanding mechanisms of MOC collapse and recovery is the documentation of upper ocean hydrographic changes in the vicinity of North Atlantic deep convection sites. Here we present new high-resolution ocean temperature and $\delta^{18}O_{sw}$ records spanning the last deglaciation from an eastern subpolar North Atlantic site that lies along the flow path of the North Atlantic Current, approaching deep convection sites in the Labrador and Greenland-Iceland-Norwegian (GIN) Seas. High-resolution temperature and $\delta^{18}O_{sw}$ records from subpolar Site 980 help track the movement of the subpolar/subtropical front associated with temperature and Atlantic MOC changes throughout the last deglaciation. Distinct $\delta^{18}O_{sw}$ minima during Heinrich-1 (H1) and the Younger Dryas (YD) correspond with peaks in ice-rafted debris and periods of reduced Atlantic MOC, indicating the presence of melt water in this region that could have contributed to MOC reductions during these intervals. Increased tropical and subtropical $\delta^{18}O_{sw}$ during these periods of apparent freshening in the subpolar North Atlantic suggest a buildup of salt at low latitudes that served as a negative feedback on reduced Atlantic MOC.

1. Introduction

The Atlantic meridional overturning circulation (MOC) is strongly dependent on the densification of surface waters that occurs as warm, salty subtropical waters feeding the North Atlantic Current give up heat as they flow eastward across the Atlantic Basin north of 45°N (Fig. 1). The surface ocean circulation pattern in the subpolar North Atlantic distributes these dense waters to the Labrador and Greenland-Iceland-Norwegian (GIN) Seas where North Atlantic Deep Water (NADW), a critical component of the MOC, is formed. Changes in the North Atlantic freshwater budget due to melting continental ice sheets and icebergs may have disrupted the MOC (Stocker et al., 1992; Manabe and Stouffer, 1997). Widespread paleoclimatic evidence suggests that the last deglaciation was marked by large, abrupt changes in temperature and Atlantic MOC (Boyle and Keigwin, 1987; Vidal et al., 1997; McManus et al., 2004; Robinson et al., 2005). Mechanisms underlying Atlantic MOC recovery throughout climate history remain unclear, particularly the rapid recovery at the onset of the Bølling. Recent paleoceanographic studies (Schmidt et al., 2004; Carlson et al., 2008; Schmidt et al., 2006) describe a self-sustaining negative feedback mechanism by which the slowdown of MOC causes a gradual buildup of salt in the tropical/subtropical Atlantic that gradually preconditions the North Atlantic for an increase in surface water density and subsequent MOC recovery. This occurs via advection of salt into the GIN and Labrador Seas until threshold density is reached, hence the abrupt return to “on” mode. Model simulations have also shown evidence of another mechanism for low latitude salt buildup involving a feedback between Atlantic MOC and Intertropical Convergence Zone (ITCZ) dynamics

(Vellinga and Wood, 2002; Dahl et al., 2005; Zhang and Delworth, 2005). Recent studies (Thornalley et al., 2009; Thornalley et al., 2010) support an alternative negative feedback based on the hypothesis of Clark et al. (2001), whereby during periods of enhanced melt water release into the subpolar North Atlantic (and associated reductions in Atlantic MOC and cooling), the expansion of the Laurentide Ice Sheet cuts off melt water discharge routes, causing the inflow to deep convection sites via the subpolar gyre to become more saline and eventually restore deep convection.

Previous North Atlantic reconstructions based on pairing $\delta^{18}O_c$ (oxygen isotope composition of foraminiferal calcite relative to the standard Vienna Pee Dee Belemnite, or VPDB) and transfer function temperatures have shown evidence of reduced upper ocean salinity during glacial (Cortijo et al., 1997) and deglacial (Duplessy et al., 1992) ice rafting events. More recent multi-species $\delta^{18}O_c$ and Mg/Ca temperature reconstructions spanning the last deglaciation from the northeastern Atlantic (Peck et al., 2008) and just south of Iceland (Thornalley et al., 2010) also show evidence of melt water influence on surface hydrography that likely contributed to deglacial Atlantic MOC disruptions (McManus et al., 2004).

Here, we present new high-resolution planktonic foraminiferal temperature and $\delta^{18}O_{sw}$ (oxygen isotope composition of seawater relative to Standard Mean Ocean Water, or SMOW) reconstructions with accompanying ice-rafted debris (IRD) (McManus et al., 1999) spanning the last deglaciation. These records document millennial-scale variability of upper ocean temperature, salinity, and iceberg activity in the northeastern Atlantic,

providing further insight into links between North Atlantic upper ocean salinity, iceberg melt water, and abrupt MOC changes of the last deglaciation.

2. Regional Setting

Sediments for this study were recovered from Ocean Drilling Program (ODP) Site 980 (55°29'N, 14°42'W, 2179 m) located on the Feni Drift in the eastern subpolar North Atlantic (Fig. 1). Warm, salty subtropical waters feed the North Atlantic Current, which moves eastward across the Atlantic Basin north of 45°N, giving up its heat along the way and delivering dense (cold, salty) water to deep convection sites of the polar North Atlantic. Surface waters at Site 980 lie directly in the path of the North Atlantic Current at the boundary between warm, salty subtropical and cold subpolar waters, just to the north of a major North American iceberg trajectory driven by a cyclonic surface gyre, and are thus highly sensitive to regional climate changes (McManus et al., 1999). Sediments from Site 980 contain ice-rafted detritus (IRD) from eastern North America, Greenland, and Iceland (Bond et al., 1997). Although the majority of 980 IRD is thought to originate from the Laurentide, Greenland, and Iceland ice sheets, this site's proximity to the British ice sheet might also make it sensitive to NW European ice sheet instabilities during the last deglaciation (Peck et al., 2006).

3. Materials and Methods

Sedimentation rates spanning the interval of interest (~10-22 ka) average 23 cm ky^{-1}, and sampling at 1-4 cm intervals provides centennial- to millennial-scale resolution. The

chronology is based on 35 calibrated ^{14}C ages (Table 1). Paired geochemical measurements of two planktonic foraminifer species, *Neogloboquadrina pachyderma* (dextral (d), or right-coiling) and *Neogloboquadrina pachyderma* (sinistral (s), or left-coiling), constrain changes in upper ocean temperature and salinity and their relationship to global climate and deep ocean circulation. The oxygen isotope composition of foraminiferal calcite ($\delta^{18}O_c$) reflects both ambient calcification temperature and seawater isotopic composition ($\delta^{18}O_{sw}$). Independent estimates of calcification temperature from Mg/Ca measurements differentiate temperature and $\delta^{18}O_{sw}$ influences on $\delta^{18}O_c$.

Although both the left- and right-coiling varieties are observed in subpolar North Atlantic waters, *N. pachyderma* (s) geochemistry typically reflects colder temperatures than *N. pachyderma* (d). In ice-free areas, *N. pachyderma* is typically found at depths of 100 m or below (Bé, 1977), whereas under conditions of cooling and increased ice cover, its habitat may shift to shallower depths (Carstens et al., 1997). A recent data set from the Norwegian Sea (Nyland et al., 2006) suggests that during summer months, *N. pachyderma* (d) calcifies in the thermocline at ~50 m, whereas *N. pachyderma* (s) calcifies at depths of 100 m and deeper. At Site 980, temperatures at 100 m and deeper are not highly variable throughout the year, whereas mixed layer warming and stratification during summer months produces seasonal variations in the upper ~50-75 m (Boyer et al., 2009).

3.1 Stable Isotopes

Isotope measurements were made at 1-3 cm intervals in ODP 980. Specimens of *N. pachyderma* (d) and *N. pachyderma* (s) were picked from the 150-250 μm size fraction. 7 (s) to 10 (d) specimens were loaded for each stable isotope measurement. In preparation for stable isotope analysis, samples were cracked and sonicated in methanol and dried at 70°C. Samples were analyzed at Woods Hole Oceanographic Institution on a Finnigan-MAT 253 stable isotope ratio mass spectrometer coupled to a Kiel III carbonate device. Samples were reacted at 70°C in phosphoric acid. Standard deviation of National Bureau of Standards (NBS) carbonate standard NBS-19 is 0.07 permil and 0.03 permil for $\delta^{18}O$ and $\delta^{13}C$, respectively. Data were calibrated to Pee Dee Belemnite (PDB) using the NBS-19 standard.

3.2 Mg/Ca

Mg/Ca ratios were measured on *N. pachyderma* (d) and *N. pachyderma* (s) (average starting sample sizes of ~500-600 μg when available). Samples were delicately cracked open between two glass slides and cleaned using published trace metal techniques (Boyle and Keigwin, 1985/1986) with a reversal of the oxidative and reductive cleaning steps (Rosenthal et al., 1995). Samples were dissolved in 5% HNO_3 (trace metal-grade), and Mg/Ca ratios were measured on a Thermo-Finnigan Element 2 sector field single collector ICP-MS (Rosenthal et al., 1999). Mn/Ca and Al/Ca measurements served as monitors of contamination from diagenetic and detrital sources, respectively. An external 50-ppm Ca standard was used to convert ICP-MS intensity ratios to elemental ratios. We

corrected for matrix effects by running a series of samples with the same Mg/Ca but varying [Ca]. Analytical precision was calculated from three consistency standards (measured as samples twice during the course of each run) of varying Mg/Ca (1.7-5.0 mmol mol^{-1}). Calcification temperature was calculated from Mg/Ca using species-specific calibration equations for *N. pachyderma* (d) (Eq. 1, von Langen et al., 2005) and *N. pachyderma* (s) (Eq. 2, Elderfield and Ganssen, 2000). $\delta^{18}O_{sw}$ was calculated from a *N. pachyderma* paleotemperature equation (Eq. 3, von Langen et al., 2000; Bemis et al., 2002).

Equation 1. $Mg/Ca = 0.51 * \exp^{(0.10*Temperature)}$ (*N. pachyderma* (dextral))

Equation 2. $Mg/Ca = 0.52 * \exp^{(0.10*Temperature)}$ (*N. pachyderma* (sinistral))

Equation 3. $T\ (°C) = 17.3 - 6.07 * (\delta^{18}O_c - \delta^{18}O_w)$ (*N. pachyderma*)

3.3 MAT

For each faunal sample, we generated quantitative warm and cold season surface temperature (SST) estimates from planktonic foraminiferal assemblage changes using the Modern Analog Technique (MAT) (Prell, 1985) and the Brown University core-top database (Prell et al., 1999). Sediment samples were dry-sieved at 150 μm and then split to give approximately 300 planktonic foraminifera for census counts. Forty-one species of planktonic foraminifera were identified, if present. The actual number of planktonic foraminifera counted in a sample ranged from 235 to 695 specimens with an average of 394 specimens during the deglacial interval. For the MAT SST estimates, we used the average temperature of the best ten analogs from the North Atlantic Ocean.

3.4 Sea Level Correction

Coral-based records of changing global sea level provide reasonable corrections for the component of $\delta^{18}O_{sw}$ change caused by global ice volume variations. We applied an ice volume correction to our $\delta^{18}O_{sw}$ records using the coral-based sea level reconstruction of Clark and Mix (2002), assuming a $\delta^{18}O_{sw}$-sealevel scaling of 0.0075 ‰ m^{-1} decrease in relative sea level (RSL) (Schrag et al., 2002).

3.5 Chronology

The chronology for ODP Site 980 is based on 35 monospecific foraminifera accelerator mass spectrometry (AMS) ^{14}C dates (*G. bulloides, N. pachyderma* (d), *N. pachyderma* (s)) spanning from the LGM to the late Holocene (Table 1). The Calib (Stuiver and Reimer, 1993) program (version 6.0, Marine09 calibration data set of Reimer et al., 2009) was used to convert ^{14}C ages to calendar ages. The resulting age model suggests an average sedimentation rate of ~23 cm ky^{-1} throughout the deglacial interval. Calendar age differences between *N. pachyderma* (s) and *N. pachyderma* (d) at the same depths (Table 1) are mostly on the order of 100-200 years, except for a ~900-year difference just prior to the onset of the BA, which may reflect age differences in polar vs. subpolar water masses. These age discrepancies are taken into account by applying slightly different age models for *N. pachyderma* (s) vs. *N. pachyderma* (d) records (based on dual ages obtained at the four depth intervals listed in Table 1).

We assumed a reservoir age of 400 years, except for the YD, H1, and post-H1 intervals, which were identified by the 980 IRD record. We applied reservoir ages of 800 years (Bard et al., 1994; Austin et al., 1995) for the YD interval and 1,500-2,000 years (Peck et al., 2006) across the H1/post-H1 interval. Peck et al. (2006) report reservoir ages of ~1,500 years at the height of H1 and 2,000 years immediately following H1 during the period of reduced Atlantic MOC (McManus et al., 2004). We identified this period of reduced MOC at Site 980 using the benthic $\delta^{13}C$ record, which is low in resolution but provides a reasonable constraint on the recovery of the Atlantic MOC prior to the onset of the Bølling warm period. Peck et al. (2006) provide one of the few estimates of H1/post-H1 reservoir ages for the North Atlantic, and their site is close to Site 980, so we are confident that these represent reasonable reservoir ages for these intervals.

3.6 Error Analysis

Analytical precision of $\delta^{18}O_c$ based on replicate analyses of NBS-19 is ±0.07 ‰. Analytical precision for Mg/Ca based on replicate analyses of three consistency standards of varying Mg/Ca (1.7-5.0 mmol mol^{-1}) is 0.04 mmol/mol. This translates to an average temperature error of 0.4°C over the observed temperature ranges shown by *N. pachyderma* (d and s) in this study. The error introduced by the Mg/Ca-temperature calibration equations is 0.6°C for *N. pachyderma* (s) (Elderfield and Ganssen, 2000) and 1.0°C for *N. pachyderma* (d) (von Langen et al., 2005). The combined analytical and calibration error for Mg/Ca is 0.7°C for *N. pachyderma* (s) and 1.1°C for *N. pachyderma*

(d), so we apply an average total Mg/Ca error of 0.9°C here. Based on these errors for Mg/Ca temperature and $\delta^{18}O_c$, and assuming a 1σ normal distribution in Mg/Ca and $\delta^{18}O_c$, the compounded $\delta^{18}O_{sw}$ error is ±0.22 ‰. It is important to note that the calibration range for the paleotemperature equation (Eq. 3, von Langen et al., 2000; Bemis et al., 2002) is based on a calibration temperature range of 9-19°C. The full range of estimated deglacial temperatures at Site 980 from both *N. pachyderma* (d) and *N. pachyderma* (s) is significantly larger than that, which may represent an additional source of error.

4. Results

4.1 $\delta^{18}O_{calcite}$ Results

The *N. pachyderma* (d) and *N. pachyderma* (s) $\delta^{18}O_c$ records show similar patterns of variability over the last 22 ky. $\delta^{18}O_c$ maxima occur during the LGM followed by a ~1.5-2.0 permil deglacial decrease (Fig. 2). The $\delta^{18}O_c$ values of the two species overlapped during the LGM, which could suggest reduced seasonality or a less stratified water column. Peck et al. (2008) observe a similar $\delta^{18}O_c$ overlap between *G. bulloides* and *N. pachyderma* (s) during this interval that suggests a less stratified water column. Alternatively, the LGM convergence of *N. pachyderma* (d) and *N. pachyderma* (s) $\delta^{18}O_c$ may suggest that the *N. pachyderma* (d) specimens from this interval are actually right-coiling variants of *N. pachyderma* (s), as observed in modern specimens from polar regions with a low relative abundance of *N. pachyderma* (d) (Bauch et al., 2003). During

the deglaciation, lower $\delta^{18}O_c$ of *N. pachyderma* (d) relative to *N. pachyderma* (s) likely reflects warmer temperature preferences related to depth habitat or seasonality.

Based on $\delta^{18}O$ and Mg/Ca data from the Norwegian Sea, Nyland et al. (2006) observed a disequilibrium offset in the oxygen isotope composition of both *N. pachyderma* (s) and *N. pachyderma* (d) associated with post-gametogenic processes. In Figs. 2-4 (see alternative scales), we show our $\delta^{18}O_c$ and $\delta^{18}O_{sw}$ records with a disequilibrium offset of +0.6 permil (Nyland et al., 2006 and references within).

4.2 Mg/Ca and MAT Results

Although *N. pachyderma* (s) is present throughout the duration of the deglaciation, *N. pachyderma* (d) abundance decreases prior to H1, so there were not enough specimens available for Mg/Ca analysis. The *N. pachyderma* (d) and *N. pachyderma* (s) Mg/Ca records yield quite different deglacial temperature patterns and amplitudes. The *N. pachyderma* (d) temperatures exhibit a range of ~8°C and higher amplitude variability (~3-4°C) than *N. pachyderma* (s) throughout the deglaciation. *Neogloboquadrina pachyderma* (d) temperature trends are somewhat similar to those over Greenland (Grootes and Stuiver, 1997), except for a slightly earlier (relative to GISP2) temperature increase at 980 of ~3-4 °C just prior to the onset of the Bølling warm period, and a slightly delayed (relative to GISP2) ~3°C temperature decrease at site 980 associated with the YD.

The *N. pachyderma* (s) Mg/Ca record yields much lower amplitude (~1-2°C) deglacial temperature variability. Both MAT and *N. pachyderma* (s) temperatures

increase between the LGM and the Bølling-Allerød (BA) period, with continued warming across the Heinrich-1 (H1) interval. Apart from the interval between 12-16 ky BP (*N. pachyderma* (s)), both *N. pachyderma* (d and s) Mg/Ca temperature records fall within reasonable range of independent, lower resolution Modern Analog Technique (MAT)-derived summer and winter temperatures at Site 980 (Fig. 2). Apart from the onset of the BA, the MAT summer temperatures are warmer than the Mg/Ca temperatures throughout much of the record, consistent with *N. pachyderma* being less prevalent in the warm seasonal assemblage.

The full range of deglacial MAT and Mg/Ca temperatures observed at Site 980 is ~0-13°C (Fig. 2). The modern annual average temperature at Site 980 (50-100 m) is ~10-11°C with a seasonal range of ~10-13°C (Boyer et al., 2009). The upper 200 m of the water column is isothermal during winter months, and spring stratification develops at ~25-50 m, strengthening throughout the summer months and then weakening again in the Fall. The modern seasonal temperature range is consistent with the observed range of Mg/Ca temperature variability immediately following the YD period.

Previous culture studies (Lea et al., 1999; Nürnberg et al., 1996) indicate only a minor effect of salinity (relative to temperature) on Mg/Ca. However, more recent studies (Kısakürek et al., 2008; Ferguson et al., 2008) suggest that salinity effects on Mg/Ca may be significant enough to incorporate into calibration equations, particularly in high salinity regions. The modern annual average salinity at Site 980 at ~50-100 m is 35.40-35.45 PSU with seasonal variability of <0.10 PSU, and measured Mg/Ca temperatures for both *N. pachyderma* (d) and *N. pachyderma* (s) fall within reasonable range of

independently derived MAT temperatures and in some cases are even lower, suggesting that the Mg/Ca temperature proxy is not biased (to higher values) by high salinities.

4.3 $\delta^{18}O_{sw}$ Results

Removal of local Mg/Ca temperature and global ice volume (Clark and Mix, 2002) effects on *N. pachyderma* (d and s) $\delta^{18}O_c$ yields an estimate of upper ocean $\delta^{18}O_{sw}$ (Fig. 3), which likely reflects local salinity and hydrological changes. *Neogloboquadrina pachyderma* (s) $\delta^{18}O_{sw}$ increases toward the end of the LGM, interrupted by a ~1.0-permil decrease at the onset of H1. Following H1, *N. pachyderma* (s) $\delta^{18}O_{sw}$ gradually increases, reaching ~0.7-0.8 permil during the BA, slightly lower than pre-H1 values. The *N. pachyderma* (s) $\delta^{18}O_{sw}$ remains constant across the BA, including Meltwater Pulse 1a (MWP-1a, 13.7-14.2 ky BP, Stanford et al., 2006), and into the YD with only minor variability during the second half of the YD.

Neogloboquadrina pachyderma (d) $\delta^{18}O_{sw}$ minima occur in conjunction with the two ice rafting events of the last deglaciation, H1 and YD. Following H1, the $\delta^{18}O_{sw}$ recovers rapidly, approaching a maximum of ~0.9-1.0 permil at the onset of the BA. The *N. pachyderma* (d) $\delta^{18}O_{sw}$ shows variations of up to ~0.5 permil across the BA interval, including MWP-1a. $\delta^{18}O_{sw}$ values decrease by almost 1.0 permil during the YD and then recover to values observed during the BA, but with slightly larger (>0.5 permil) variability. Though highly variable, BA and post-YD $\delta^{18}O_{sw}$ are comparable to modern $\delta^{18}O_{sw}$ at this location (LeGrande and Schmidt, 2006).

It is difficult to quantify salinity changes due to uncertainties surrounding the $\delta^{18}O_{sw}$-S relationship in the North Atlantic, which is unlikely to be stable through time. Based on the modern regional $\delta^{18}O_{sw}$-S (LeGrande and Schmidt, 2006), which is dominated by local hydrological conditions (E-P), the largest $\delta^{18}O_{sw}$ changes correspond to salinity changes of ~2.6 PSU for *N. pachyderma* (d) (H1 to BA) and ~1.8 PSU for *N. pachyderma* (s) (end of LGM to H1). However, during deglaciation, the presence of glacial melt water likely steepened the slope of the $\delta^{18}O_{sw}$-S (Cortijo et al., 1997), thus reducing the amplitudes of associated salinity variations. A doubling of the slope would yield salinity changes that were approximately half of those listed above.

5. Discussion

5.1 Deglacial Changes in the North Atlantic: The Polar Front, Melt Water, and the Atlantic MOC

The *N. pachyderma* (s) and *N. pachyderma* (d) Mg/Ca records yield very different deglacial temperature patterns. *Neogloboquadrina pachyderma* (s) temperatures are lowest during the LGM and increase gradually throughout the first half of the deglaciation and then level out during the BA and YD intervals (Fig. 2), whereas *N. pachyderma* (d) temperatures are more variable. Unlike $\delta^{18}O_{sw}$ records, which are offset during cold intervals (H1, YD) but overlap during warm intervals (BA), the Mg/Ca and $\delta^{18}O_c$ records for the two species remain offset throughout much of the deglaciation. As suggested earlier, these geochemical offsets may reflect different seasonal preferences or depth habitats. In the case of seasonal preferences, *N. pachyderma* (s) might represent

winter conditions with muted variability associated with increased sea ice cover relative to summer months when *N. pachyderma* (d) is more prevalent. Alternatively, if the temperature offset between the two species reflects different depth habitats, the higher and more variable *N. pachyderma* (d) temperatures are consistent with a shallower depth habitat, whereas *N. pachyderma* (s) temperatures reflect the smaller temperature changes expected in deeper waters (>100 m), which exhibit little to no seasonal temperature variability today (Boyer et al., 2009). In this scenario, $\delta^{18}O_{sw}$ overlap between *N. pachyderma* (d) and *N. pachyderma* (s) during warmer intervals (BA, post-YD) likely indicates a greater influence of warm, salty subtropical water from the south associated with a stronger Atlantic MOC, whereas $\delta^{18}O_{sw}$ offsets between *N. pachyderma* (d) and *N. pachyderma* (s) during cold ice rafting events (H1 and YD) may indicate the presence of a strong melt water-driven halocline. The warming that precedes both ice-rafting events (*N. pachyderma* (s) from ~19.0-16.7 ky BP, *N. pachyderma* (d) at ~13.0-12.5 ky BP) sets the stage for increased melt water input and subsequent halocline development.

The observed deglacial $\delta^{18}O_{sw}$ differences between warm (BA) and cold (H1, YD) intervals span a range of 0.6-1.5 permil, which is comparable to the subpolar-subtropical $\delta^{18}O_{sw}$ gradient in the modern North Atlantic (~1.0 permil) (LeGrande and Schmidt, 2006), supporting the idea that $\delta^{18}O_{sw}$ variability at Site 980 (Figs. 2 and 3) was strongly influenced by changes in the position of the subpolar/subtropical front. Co-occurrence of planktonic foraminiferal $\delta^{18}O_{sw}$ minima with peaks in IRD during H1 and the YD (Fig. 3) strongly supports local freshening associated with melt water at Site 980. Approximately 1-permil decreases in *N. pachyderma* (s) $\delta^{18}O_{sw}$ across H1 and *N. pachyderma* (d) $\delta^{18}O_{sw}$

across YD translate to salinity decreases of ~1.7 PSU based on the modern regional $\delta^{18}O_{sw}$-S from LeGrande and Schmidt (2006). Consistent with its closer vicinity to the coast (and British ice sheet), nearby site MD01-2461 shows a freshening of up to 2.6 PSU across H1 (Peck et al., 2006). Cortijo et al. (1997) did not observe freshening north of 50°N during glacial ice rafting events, which may reflect differences in the positioning of the subpolar/subtropical front and associated variations in sea ice cover and surface ocean circulation patterns between glacial and deglacial climate states (Sarnthein et al., 1995).

The lack of IRD at Site 980 during MWP-1a rules out the presence of local iceberg melt water in this region of the subpolar North Atlantic at that time (Fig. 3). The *N. pachyderma* (s) Mg/Ca temperatures and $\delta^{18}O_{sw}$ are stable across this interval, but *N. pachyderma* (d) is more variable with millennial-scale shifts between warmer/saltier (subtropical) and colder/fresher (subpolar) conditions, suggesting high-frequency changes in the positioning of the subpolar/subtropical front. Despite the lack of IRD, this region may have received minor local inputs of melt water from the British ice sheet during this interval, perhaps only enough to impact shallower dwelling (or warm season-loving) *N. pachyderma* (d). The large volume of continentally derived melt water associated with the sea level rise that accompanied MWP-1a did not seem to strongly impact MOC (McManus et al., 2004), suggesting that either the origin of melt water did not lie in the northern hemisphere (Clark et al., 2002), or the location and depth distribution of Laurentide ice sheet melt water injection may have a larger impact on MOC than melt water volume (Stanford et al., 2006).

Decreases in benthic $\delta^{13}C$ at Site 980 and increases in $^{231}Pa/^{230}Th$ in the deep (>3,000 m) western Atlantic (McManus et al., 2004) (Fig. 3), as well as the deep eastern Atlantic (Gherardi et al., 2005), suggest reduced Atlantic MOC during cold intervals of the last deglaciation (H1, YD) that were likely driven by melt water input and subsequently reduced upper ocean densities at or near sites of deep convection. IRD maxima and $\delta^{18}O_{sw}$ minima at Site 980 during both H1 and YD correspond with the observed decreases in Atlantic MOC, suggesting that melt water in this region could have contributed to the freshening that slowed the MOC. Nearby site MD01-2461 (Peck et al., 2006) shows similar IRD peaks for H1 and H2, accompanied by reduced upper ocean density and benthic $\delta^{13}C$.

A $\delta^{18}O_{sw}$ increase immediately following H1 corresponds with an initial benthic $\delta^{13}C$ increase at Site 980 (2,179 m), suggesting a reduction in melt water input to the upper ocean and the beginning of MOC recovery. However, the resumption of Atlantic MOC registered by deep (>3,000 m) $^{231}Pa/^{230}Th$ records in the western (McManus et al., 2004) and eastern (Gherardi et al., 2005) Atlantic does not begin until ~1-2 ky later. A possible explanation is that the post-H1 MOC recovery occurred in stages, with the earlier initiation of a shallower overturning circulation (Robinson et al., 2005; Carlson et al., 2008). A recent $^{231}Pa/^{230}Th$ compilation from an Atlantic depth transect (Gherardi et al., 2009) indicates that despite a reduction in deep overturning, a shallower intermediate circulation (Glacial North Atlantic Intermediate Water (GNAIW)) persisted throughout the LGM and the entire deglaciation. Although these data show reduced intermediate depth circulation (2,000-3,000 m) during H1, it does not shut down.

The average $\delta^{18}O_{sw}$ across the LGM (*N. pachyderma* (s)) is ~1.4 permil (with disequilibrium offset of +0.6 permil applied), which is in good agreement with estimates just south of Iceland (Thornalley et al., 2010). The modern regional $\delta^{18}O$-S (LeGrande and Schmidt, 2006) yields an average LGM salinity that is ~1.5 PSU higher than the modern upper ocean (50-100 m), whereas a doubling of the LeGrande and Schmidt (2006) $\delta^{18}O$-S slope (due to increased melt water influence, as suggested by LGM IRD pulses) would yield LGM salinities that were ~1.0 PSU lower than those of today. Slightly reduced salinities, in combination with the coldest temperatures in this reconstruction, may have yielded waters dense enough to support GNAIW formation.

5.2 Links to the Tropics and Subtropics

A comparison of deglacial $\delta^{18}O_{sw}$ records from Site 980 with tropical and subtropical $\delta^{18}O_{sw}$ records (Fig. 4) provides preliminary insight into potential feedbacks between high and low latitudes that may have contributed to deglacial Atlantic MOC and climate changes. The upper ocean $\delta^{18}O_{sw}$ decrease at Site 980 occurs in conjunction with the MOC collapse at the onset of the Oldest Dryas period ~18-19 ky BP, and is accompanied by an increase in $\delta^{18}O_{sw}$ (Fig. 4) in the tropical Atlantic (Schmidt et al., 2004) and Pacific (Benway et al., 2006) (Fig. 4), as well as the subtropical Atlantic (Carlson et al., 2008). Between H1 and the BA onset, increasing $\delta^{18}O_{sw}$ at Site 980 is accompanied by decreasing tropical and subtropical $\delta^{18}O_{sw}$ (Fig. 4). While subpolar North Atlantic $\delta^{18}O_{sw}$ is higher throughout the BA, tropical and subtropical $\delta^{18}O_{sw}$ are lower during this period.

A decrease in *N. pachyderma* (d) $\delta^{18}O_{sw}$ during the YD corresponds with increasing tropical and subtropical $\delta^{18}O_{sw}$.

A gradual build-up of salt in the tropics and subtropics has been proposed as a self-limiting negative feedback mechanism for restoring Atlantic MOC (Schmidt et al., 2004; Carlson et al., 2008; Schmidt et al., 2006). During the Oldest Dryas interval when MOC is hypothesized to have reduced dramatically (McManus et al., 2004), an active overturning circulation at intermediate depths in the North Atlantic, as evidenced by intermediate-depth coral ^{14}C (Robinson et al., 2005) and sedimentary $^{231}Pa/^{230}Th$ data (Hall et al., 2006; Gherardi et al., 2009), may have gradually increased the salt content of North Atlantic surface waters at deep convection sites until a threshold salinity was achieved, triggering the abrupt resumption of MOC at the onset of the BA warm period.

Alternatively, a low latitude feedback on Atlantic MOC involving Intertropical Convergence Zone (ITCZ) dynamics has been simulated in numerous models, whereby during periods of high-latitude cooling and reduced MOC, general circulation model (GCM) simulations show a southward migration of the ITCZ (Vellinga and Wood, 2002; Dahl et al., 2005; Zhang and Delworth, 2005), resulting in high net evaporation (E-P) over the northern tropics. Enhanced evaporation promotes the build-up of salt in the tropical and subtropical Atlantic. Stronger winds in the northern tropics that accompany a southward displacement of the ITCZ may exacerbate Atlantic salt build-up by increasing Atlantic-Pacific water vapor transport (Benway et al., 2006; Leduc et al., 2007).

The observed $\delta^{18}O_{sw}$ increases at tropical/subtropical sites relative to reduced subpolar $\delta^{18}O_{sw}$ (H1, YD) supports an increase in tropical/subtropical salinity during

periods of reduced Atlantic MOC. However, the collective chronological uncertainties of these records preclude any definitive statements regarding the relative timing of millennial-scale low- vs. high-latitude changes.

6. Conclusions

A growing network of paleoceanographic records from the Atlantic basin confirms the importance of Atlantic MOC in millennial-scale temperature and salinity variations of the last deglaciation. High-resolution temperature and $\delta^{18}O_{sw}$ records from subpolar North Atlantic Site 980 track the movement of the subpolar/subtropical front associated with temperature and Atlantic MOC changes throughout the last deglaciation. The co-occurrence of planktonic foraminiferal $\delta^{18}O_{sw}$ minima with peaks in IRD and % *N. pachyderma* (s) during H1 and the YD (Figs. 2 and 3) strongly supports the presence of melt water at Site 980 that likely came from ice bergs, the majority of which likely originated from the Laurentide, Greenland, and Iceland ice sheets (Bond et al., 1997). IRD maxima and $\delta^{18}O_{sw}$ minima during H1 and YD correspond with decreases in benthic $\delta^{13}C$ at Site 980 and increases in $^{231}Pa/^{230}Th$ in the deep (>3,000 m) Atlantic basin (McManus et al., 2004; Gherardi et al., 2005), suggesting that melt water in this region may have contributed to reduced MOC during these intervals. Increased tropical/subtropical $\delta^{18}O_{sw}$ during periods of reduced subpolar $\delta^{18}O_{sw}$ during cold intervals with reduced MOC (H1, YD) (Fig. 4) support two hypothesized mechanisms involving low latitude salt buildup for restoring MOC at the onset of the BA, one involving an internal negative feedback and one requiring a low latitude feedback.

7. Acknowledgments

We thank W. Broecker and S. Hemming for deglacial AMS ^{14}C dates and D. Ostermann, S. Brown-Leger, L. Zou, D. Schneider, and S. Birdwhistell for laboratory assistance. We thank two anonymous reviewers for very helpful and constructive feedback on the manuscript. Support for this research was provided by the U.S. National Science Foundation (JFM and DWO) and a postdoctoral scholarship funded in part by the Gary Comer Science and Education Foundation (HB).

8. References

Austin, W. E. N., Bard, E., Hunt, J. B., Kroon, D., Peacock, J. D., 1995. The ^{14}C age of the Icelandic Vedde Ash: Implications for Younger Dryas marine reservoir age corrections. Radiocarbon 37, 53-62.

Bard, E., Arnold, M., Mangerud, M., Paterne, M., Labeyrie, L., Duprat, J., Mélières, M. A., Sonstegaard, E., Duplessy, J. C.,1994. The North Atlantic atmosphere-sea surface ^{14}C gradient during the Younger Dryas climatic event. Earth Planet. Sci. Lett. 126, 275-287.

Bauch, D., Darling, K., Simstich, J., Bauch, H.A., Erlenkeuser, H., Kroon, D., 2003. Palaeoceanographic implications of genetic variation in living North Atlantic *Neogloboquadrina pachyderma*. Nature 424, 299-302.

Bé, A. W. H., 1977. An ecological, zoogeographic and taxonomic review of recent planktonic foraminifera. In: A.T.S. Ramsay (Ed.), Oceanic Micropaleontology. Academic Press, New York, pp. 1-100.

Bemis, B. E., Spero, H. J., Thunell, R. C., 2002. Using species-specific paleotemperature equations with foraminifera: A case study in the Southern California Bight. Mar. Micropal. 46, 405-430.

Benway, H. M., Mix, A. C., Haley, B. A., Klinkhammer, G. P., 2006. Eastern Pacific Warm Pool paleosalinity and climate variability: 0-30 kyr. Paleoceanography 21, doi: 10.1029/2005PA0001208.

Bond G., Showers, W., Cheseby, M., Lotti, R., Almasi, P., deMenocal, P., Priore, P., Cullen, H., Hajdas, I., Bonani, G., 1997. A pervasive millennial-scale cycle in North Atlantic Holocene and Glacial climates. Science 278, 1257-1266.

Boyer, T. P., Antonov, J. I., Baranova, O. K., Garcia, H. E., Johnson, D. R., Locarnini, R. A., Mishonov, A. V., O'Brien, T. D., Seidov, D., Smolyar, I. V., Zweng, M. M., 2009. *World Ocean Database 2009.* S. Levitus, Ed., NOAA Atlas NESDIS 66, U.S. Gov. Printing Office, Wash., D.C., 216 pp., DVDs.

Boyle, E. A., Keigwin, L. D., 1985/1986. Comparison of Atlantic and Pacific paleochemical records for the last 215,000 years: changes in deep ocean circulation and chemical inventories. Earth Planet. Sci. Lett. 76, 135-150.

Boyle, E. A., Keigwin, L. D., 1987. North Atlantic thermohaline circulation during the past 20,000 years linked to high-latitude surface temperature. Nature 330, 35-40.

Carlson, A. E., Oppo, D. W., Came, R. E., LeGrande, A. N., Keigwin, L. D., Curry, W. B., 2008. Subtropical Atlantic salinity variability and Atlantic meridional circulation during the last deglaciation. Geology 36, 991-994.

Carstens, J., Hebbeln, D., Wefer, G., 1997. Distribution of planktic foraminifera at the ice margin in the Arctic (Fram Strait). Marine Micropaleontology 29, 257-269.

Clark, P. U., Marshall, S. J., Clarke, G. K. C., Hostetler, S. W., Licciardi, J. M., Teller, J. T., 2001. Freshwater forcing of abrupt climate change during the last glaciation, Science 293, 283–287, doi:10.1126/science.1062517.

Clark, P. U., Mix, A. C., 2002. Ice sheets and sea level of the Last Glacial Maximum. Quat. Sci. Rev. 21, 1-7.

Clark, P. U., Mitrovica, J. X., Milne, G. A., Tamisiea, M. E., 2002. Sea-level fingerprinting as a direct test for the source of global Meltwater Pulse 1a. Science 295, 2438-2441.

Cortijo, E., Labeyrie, L., Vidal, L., Vautravers, M., Chapman, M., Duplessy, J-C, Elliot, M., Arnold, M., Turon, J-L, Auffret, G., 1997. Changes in sea surface hydrology associated with Heinrich event 4 in the North Atlantic Ocean between 40° and 60°N. Earth Planet. Sci. Lett. 146, 29-45.

Dahl, K. A., Broccoli, A. J., Stouffer, R. J., 2005. Assessing the role of North Atlantic freshwater forcing in millennial scale climate variability: A tropical Atlantic perspective. Clim. Dyn. 24, 325-346.

Duplessy, J-C, Labeyrie, L., Arnold, M., Paterne, M., Duprat, J., van Weering, T.C.E., 1992. Changes in surface salinity of the North Atlantic Ocean during the last deglaciation. Nature 358, 485-488.

Elderfield, H., Ganssen, G., 2000. Past temperature and $\delta^{18}O$ of surface ocean waters inferred from foraminiferal Mg/Ca ratios. Nature 405, 442-445.

Ferguson, J. E., Henderson, G. M., Kucera, M., Rickaby, R. E. M., 2008. Systematic change of foraminiferal Mg/Ca ratios across a strong salinity gradient, Earth Planet. Sci. Lett. 265, 153-166.

Gherardi, J-M, Labeyrie, L., McManus, J. F., Francois, R., Skinner, L. C., Cortijo, E., 2005. Evidence from the Northeastern Atlantic basin for variability in the rate of the meridional overturning circulation through the last deglaciation. Earth Planet. Sci. Lett. 240, 710-723.

Gherardi, J-M, Labeyrie, L., Nave, S., Francois, R., McManus, J. F., Cortijo, E., 2009. Glacial-interglacial circulation changes inferred from $^{231}Pa/^{230}Th$ sedimentary records in the North Atlantic region. Paleoceanography 24, doi: 10.1029/2008PA001696.

Grootes, P. M., Stuiver, M., 1997. Oxygen 18/16 variability in Greenland snow and ice with 10^3 to 10^5-year time resolution. J. Geophys. Res. 102**,** 26,455-26,470.

Hall I. R., Moran, S. B., Zahn, R., Knutz, P. C., Shen, C-C., Edwards, R. L., 2006. Accelerated drawdown of meridional overturning circulation in the late-glacial Atlantic triggered by transient pre-H event freshwater perturbation. Geophys. Res. Lett. 33, doi: 10.1029/2006GL026239.

Kısakürek, B., Eisenhauer, A., Böhm, F., Garbe-Schönberg, D., Erez, J., 2008. Controls on shell Mg/Ca and Sr/Ca in cultured planktonic foraminiferan, *Globigerinoides ruber* (white). Earth Planet. Sci. Lett. 273, 260-269.

Lea, D. W., Mashiotta, T. A., Spero, H. J., 1999. Controls on magnesium and strontium uptake in planktonic foraminifera determined by live culturing. Geochim. Cosmochim. Acta 63, 2369-2379.

Leduc, G., Vidal, L., Tachikawa, K., Rostek, F., Sonzogni, C., Beaufort, L., Bard, E., 2007. Moisture transport across Central America as a positive feedback on abrupt climatic changes. Nature 445, 908-911.

LeGrande, A. N., Schmidt, G. A., 2006. Global gridded data set of the oxygen isotopic composition in seawater. Geophys. Res. Lett. 33, doi: 10.1029/2006GL026011.

Manabe, S., Stouffer, R. J., 1997. Coupled ocean-atmosphere model response to freshwater input: Comparison to Younger Dryas event. Paleoceanography 12, 321-336.

McCartney, M. S., Curry, R. G., Bezdek, H. F., 1996. North Atlantic's transformation pipeline chills and redistributes subtropical water. Oceanus 39, 19–23.

McManus, J. F., Oppo, D. W., Cullen, J. L., 1999. A 0.5-million-year record of millennial-scale climate variability in the North Atlantic. Science 283, 971-975.

McManus, J. F., Francois, R., Gherardi, J. –M., Keigwin, L. D., Brown-Leger, S., 2004. Collapse and rapid resumption of Atlantic meridional circulation linked to deglacial climate changes. Nature 428, 834-837.

Nürnberg, D., Bijma, J., Hemleben, C., 1996. Assessing the reliability of magnesium in foraminiferal calcite as a proxy for water mass temperatures. Geochim. Cosmochim. Acta 60, 803-814.

Nyland, B. F., Jansen, E., Elderfield, H., Andersson, C., 2006. *Neogloboquadrina pachyderma* (dex. and sin.) Mg/Ca and $\delta^{18}O$ records from the Norwegian Sea. Geochem. Geophys. Geosyst. 7, doi:10.1029/2005GC001055.

Oppo, D. W., McManus, J. F., Cullen, J. L., 2003. Deepwater variability in the Holocene epoch. Nature 422, 277-278.

Peck, V. L., Hall, I. R., Zahn, R., Elderfield, H., Grousset, F., Hemming, S. R., Scourse, J. D., 2006. High resolution evidence for linkages between NW European ice sheet instability and Atlantic Meridional Overturning Circulation. Earth and Planetary Science Letters 243, 476-488.

Peck, V. L., Hall, I. R., Zahn, R., Elderfield, H., 2008. Millennial-scale surface and subsurface paleothermometry from the northeast Atlantic, 55-8 ka BP. Paleoceanography 23, PA3221, doi:10.1029/2008PA001631.

Prell, W.L., 1985. The stability of low-latitude sea surface temperatures: An evaluation of the CLIMAP reconstruction with emphasis on the positive SST anomalies. US Department of Energy, Washington, DC (60p).

Prell, W., Martin, A., Cullen, J., Trend, M., 1999. The Brown University Foraminiferal Data Base, IGBP PAGES/World Data Center-A for Paleoclimatology Data Contribution Series #1999–027, NOAA/NGDC Paleoclimatology Program. Boulder Co., USA.

Reimer, P. J., Baillie, M. G. L., Bard, E., Bayliss, A., Beck, J. W., Blackwell, P. G., Ramsey, C. Bronk, Buck, C. E., Burr, G. S., Edwards, R. L., Friedrich, M., Grootes, P. M., Guilderson, T. P., Hajdas, I., Heaton, T. J., Hogg, A. G., Hughen, K. A., Kaiser, K.

F., Kromer, B., McCormac, F. G., Manning, S. W., Reimer, R.W., Richards, D. A., Southon, J. R., Talamo, S., Turney, C. S. M., van der Plicht, J., Weyhenmeyer, C. E., 2009. IntCal09 and Marine09 radiocarbon age calibration curves, 0 - 50,000 years cal BP. Radiocarbon 51, 1111-1150.

Robinson, L. F., Adkins, J. F., Keigwin, L. D., Southon, J., Fernandez, D. P., Wang, S-L., Scheirer, D. S., 2005. Radiocarbon variability in the western North Atlantic during the last deglaciation. Science 310, 1469-1473.

Rosenthal, Y., Lam, P., Boyle, E. A., Thomson, J., 1995. Authigenic cadmium enrichments in suboxic sediments: Precipitation and postdepositional mobility. Earth Planet. Sci. Lett. 132, 99-111.

Rosenthal, Y., Field, M. P., Sherrell, R. M., 1999. Precise determination of element/calcium ratios in calcareous samples using sector field inductively coupled plasma mass spectrometry. Anal. Chem. 71, 3248-3253.

Sarnthein, M., Jansen, E., Weinelt, M., Arnold, M., Duplessy, J-C, Erlenkeuser, H., Flatøy, A., Johannessen, G., Johannessen, T., Jung, S., Koc, N., Labeyrie, L., Maslin, M., Pflaumann, U., Schulz, H., 1995. Variations in Atlantic surface ocean paleoceanography, 50-80°N: A time-slice record of the last 30,000 years. Paleoceanography 10, 1063-1094.

Schmidt, M. W., Spero, H. J., Lea, D. W., 2004. Links between salinity variation in the Caribbean and North Atlantic thermohaline circulation. Nature 428, 160-163.

Schmidt, M. W., Vautravers, M. J., Spero, H. J., 2006. Rapid subtropical North Atlantic salinity oscillations across Dansgaard-Oeschger cycles. Nature 443, 561-564.

Schrag, D. P., Adkins, J. F., McIntyre, K., Alexander, J., Hodell, D. A., Charles, C., McManus, J., 2002. The oxygen isotopic composition of seawater during the last glacial maximum. Quat. Sci. Rev. 21, 331-342.

Stanford, J. D., Rohling, E. J., Hunter, S. E., Roberts, A. P., Rasmussen, S. O., Bard, E., McManus, J., Fairbanks, R. G., 2006. Timing of meltwater pulse 1a and climate responses to meltwater injections. Paleoceanography 21, doi: 10.1029/2006PA001340.

Stocker, T. F., Wright, D. G., Broecker, W. S., 1992. The influence of high-latitude surface forcing on the global thermohaline circulation. Paleoceanography 7, 529-541.

Stuiver, M., Reimer, P.J., 1993. Extended ^{14}C database and revised CALIB radiocarbon calibration program. Radiocarbon 35, 215-230.

Thornalley, D. J. R., Elderfield, H., McCave, I. N., 2009. Holocene oscillations in temperature and salinity of the surface subpolar North Atlantic. Nature 457, 711-714.

Thornalley, D. J. R., Elderfield, H., McCave, I. N., 2010. Reconstructing North Atlantic deglacial surface hydrography and its link to the Atlantic overturning circulation. Global and Planetary Change, doi:10.1016/j.gloplacha.2010.06.003.

Vellinga, M., Wood, R. A., 2002. Global climatic impacts of a collapse of the Atlantic thermohaline circulation. Clim. Change 54, 251-267.

Vidal, L., Labeyrie, L., Cortijo, E., Arnold, M., Duplessy, J-C, Michel, E., Becqué, S., van Weering, T.C.E., 1997. Evidence for changes in the North Atlantic Deep Water linked to meltwater surges during the Heinrich events. Earth Planet. Sci. Lett. 146,13-27.

von Langen, P.J., Lea, D.W., Spero, H.J., 2000. Effects of temperature on oxygen isotope and Mg/Ca values in *Neogloboquadrina pachyderma* shells determined by live culturing, *EOS Transactions* AGU. Fall Meeting Supplement.

von Langen, P. J., Pak, D. K., Spero, H. J., Lea, D. W., 2005. Effects of temperature on Mg/Ca in neogloboquadrinid shells determined by live culturing. Geochem., Geophys., Geosys. 6, doi:10.1029/2005GC000989.

Zhang, R., Delworth, T. L., 2005. Simulated tropical response to a substantial weakening of the Atlantic thermohaline circulation. J. Clim. 18, 1853-1860.

9. Table and Figure Legends

Figure 1. Map showing location of Site 980 (55° 29’ N, 14° 42’ W, 2179 m water depth). Orange/yellow arrows indicate surface currents, and blue/green arrows indicate deep currents (modified from McCartney et al., 1996). The northeastward-flowing path of the North Atlantic Current represents the approximate position of the subpolar-subtropical front today. During cold periods in climate history accompanied by periodic surges of icebergs (e.g., H1, YD) and subsequently colder, fresher upper ocean conditions and reduced Atlantic MOC, this boundary between warm subtropical and cold subpolar waters likely shifted southward.

Figure 2. Comparison of ODP Site 980 temperature proxy records with Greenland temperature record. Panels from top to bottom: **1)** Greenland air temperature reconstruction from GISP2 $\delta^{18}O_{ice}$ (Grootes and Stuiver, 1997); **2)** Site 980 % cold-loving species *N. pachyderma* (s); **3)** Site 980 temperature estimates based on Mg/Ca measurements of *N. pachyderma* (d) (black) and *N. pachyderma* (s) (grey) as compared to foraminiferal transfer functions using the Modern Analog Technique (MAT) (average summer and winter temperatures); Mg/Ca scale appears on the right axis; Mg/Ca temperature error is 1.1°C for *N. pachyderma* (d) and 0.7° for *N. pachyderma* (s); the modern seasonal temperature range (~10-13°C) at 50-100 m (Boyer et al., 2009) is indicated; **4)** $\delta^{18}O_c$ measurements of *N. pachyderma* (d) (black) and *N. pachyderma* (s) (grey). Alternate scale reflects disequilibrium offset of +0.6 permil (Nyland et al., 2006). Radiocarbon age control points are shown on the lower age axis (Table 1). YD = Younger Dryas, BA = Bølling-Allerød, MWP-1a = Melt Water Pulse 1a, H1 = Heinrich 1, LGM = Last Glacial Maximum.

Figure 3. Comparison of ODP Site 980 $\delta^{18}O_{sw}$ (salinity proxy) and IRD records with Greenland temperature and Atlantic MOC strength. Panels from top to bottom: **1)** Greenland air temperature reconstruction from GISP2 $\delta^{18}O_{ice}$ (Grootes and Stuiver, 1997); **2)** ODP Site 980 IRD record in lithics/gram (McManus et al., 1999); **3)** $\delta^{18}O_{sw}$ from *N. pachyderma* (d) and *N. pachyderma* (s). Alternate scale reflects disequilibrium offset of +0.6 permil (Nyland et al., 2006). The compounded $\delta^{18}O_{sw}$ error is 0.22 permil; the modern subpolar/subtropical $\delta^{18}O_{sw}$ gradient (~1.0 permil) is indicated; **4)**

Reconstruction of Atlantic MOC strength based on $^{231}Pa/^{230}Th$ calculated from ^{238}U activity (black) (McManus et al., 2004) and Site 980 benthic $\delta^{13}C$ (grey). Radiocarbon age control points are shown on the lower age axis (Table 1). YD = Younger Dryas, BA = Bølling-Allerød, MWP-1a = Melt Water Pulse 1a, H1 = Heinrich 1, LGM = Last Glacial Maximum.

Figure 4. Comparison of ODP Site 980 $\delta^{18}O_{sw}$ and tropical $\delta^{18}O_{sw}$ records. 1) Greenland air temperature reconstruction from GISP2 $\delta^{18}O_{ice}$ (Grootes and Stuiver, 1997); **2)** $\delta^{18}O_{sw}$ from *N. pachyderma* (d) and *N. pachyderma* (s). Alternate scale reflects disequilibrium offset of +0.6 permil (Nyland et al., 2006). **3)** Deglacial Caribbean (grey) (Schmidt et al., 2004) and eastern tropical Pacific (black) (Benway et al., 2006) $\delta^{18}O_{sw}$ records; **4)** Reconstruction of Atlantic MOC strength based on $^{231}Pa/^{230}Th$ calculated from ^{238}U activity (black) (McManus et al., 2004) and Site 980 benthic $\delta^{13}C$ (grey). Radiocarbon age control points are shown on the lower age axis (Table 1). YD = Younger Dryas, BA = Bølling-Allerød, MWP-1a = Melt Water Pulse 1a, H1 = Heinrich 1, LGM = Last Glacial Maximum.

Table 1. Chronology for Site 980. The chronology for ODP Site 980 is based on 35 monospecific foraminifera accelerator mass spectrometry (AMS) ^{14}C dates (*G. bulloides*, *N. pachyderma* (d), *N. pachyderma* (s)) spanning from the LGM to the late Holocene. The Calib (Stuiver and Reimer, 1993) program (version 6.0, Marine09 calibration data

set of Reimer et al., 2009) was used to convert ^{14}C ages to calendar ages. Calendar ages represent the maximum probability of the 2-sigma range.

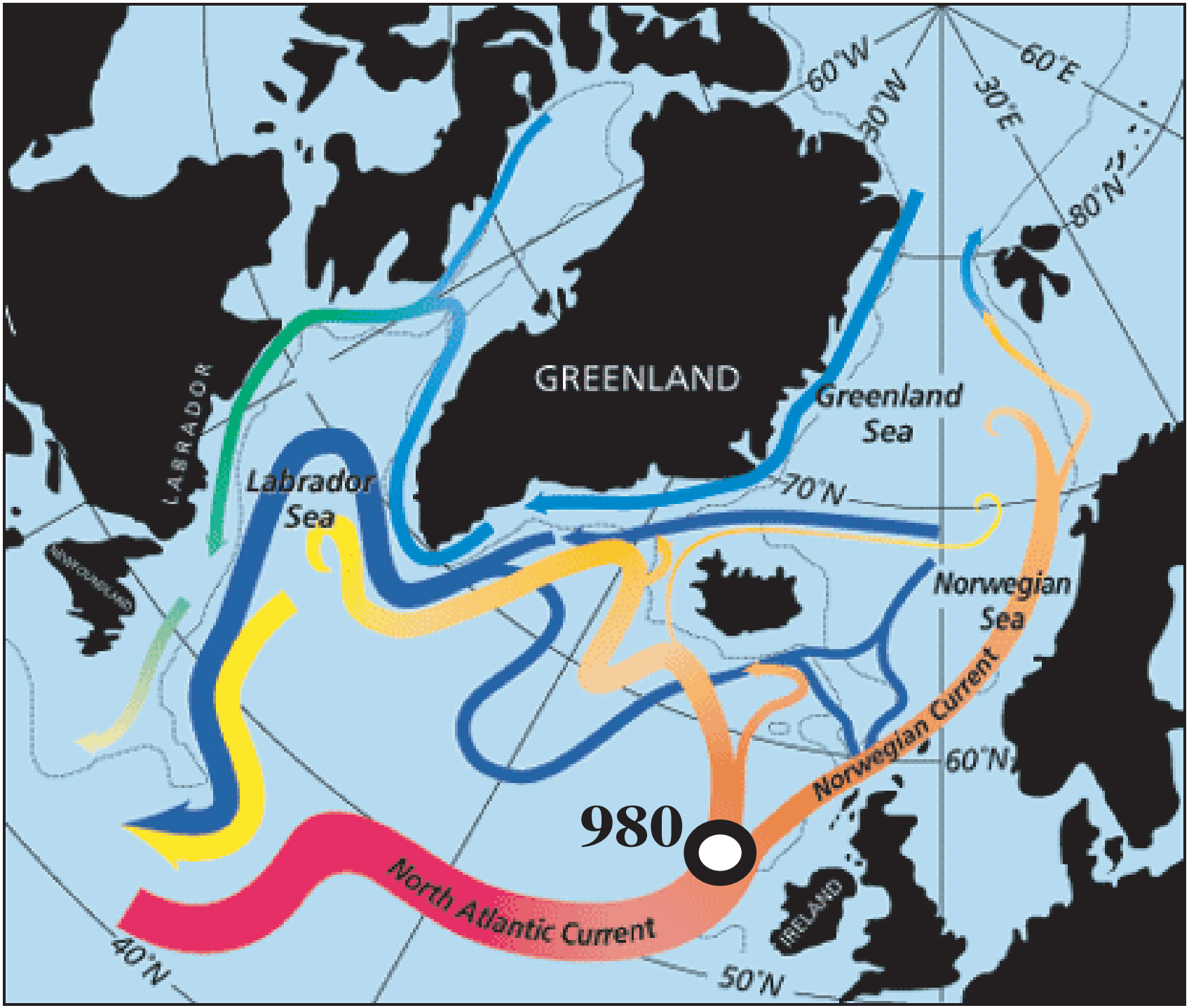
60°W
30°W
60°E
30°E
80°N
GREENLAND
Greenland Sea
LABRADOR
Labrador Sea
70°N
Norwegian Sea
Norwegian Current
60°N
980
North Atlantic Current
IRELAND
40°N
50°N

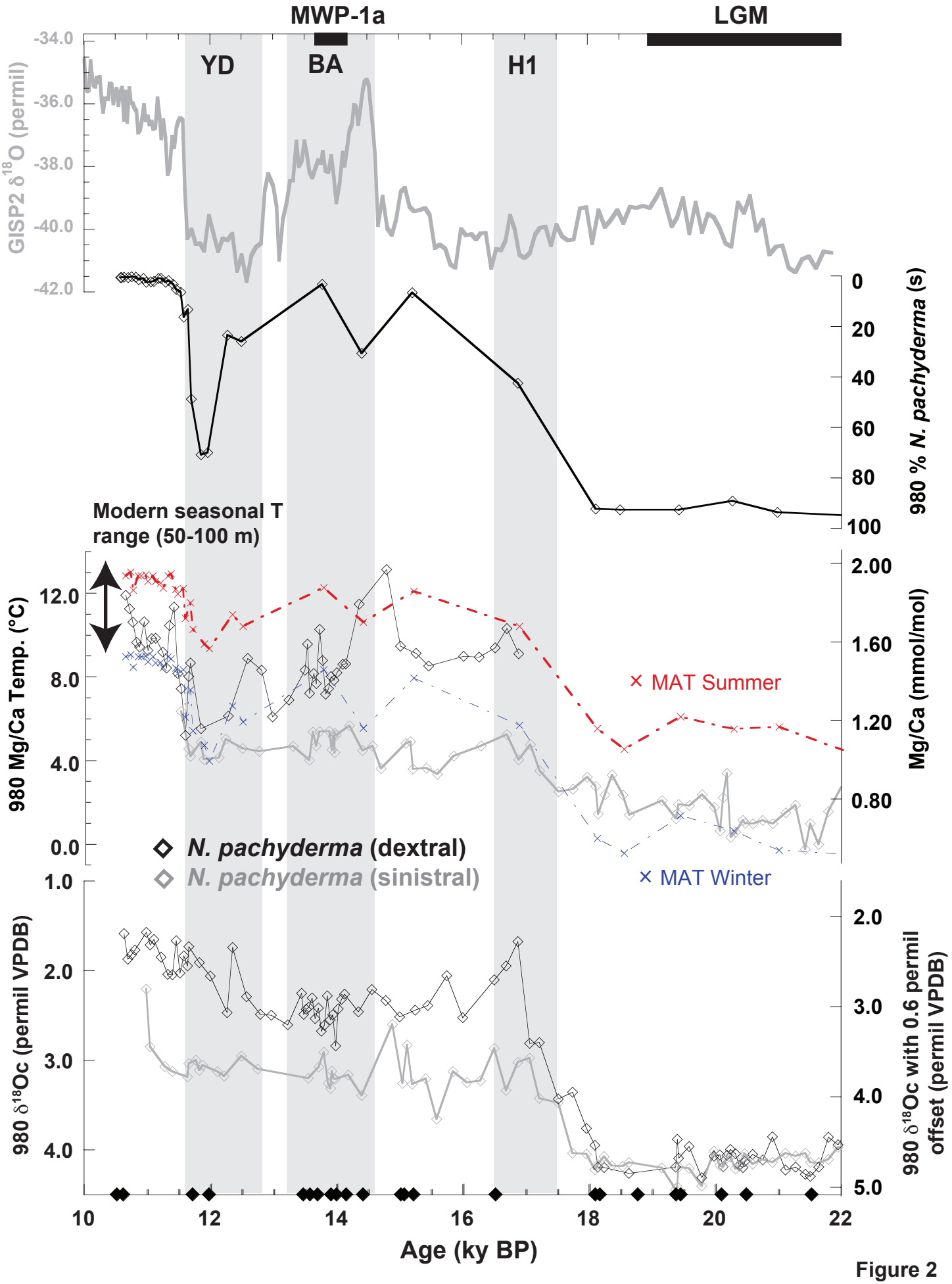
MWP-1a
LGM
YD
BA
H1
GISP2 δ18O (permil)
-34.0
-36.0
-38.0
-40.0
-42.0
0
20
40
60
80
100
980 % N. pachyderma (s)
Modern seasonal T range (50-100 m)
980 Mg/Ca Temp. (°C)
12.0
8.0
4.0
0.0
2.00
1.60
1.20
0.80
Mg/Ca (mmol/mol)
× MAT Summer
× MAT Winter
N. pachyderma (dextral)
N. pachyderma (sinistral)
980 δ18Oc (permil VPDB)
1.0
2.0
3.0
4.0
2.0
3.0
4.0
5.0
980 δ18Oc with 0.6 permil offset (permil VPDB)
10
12
14
16
18
20
22
Age (ky BP)

Figure 2

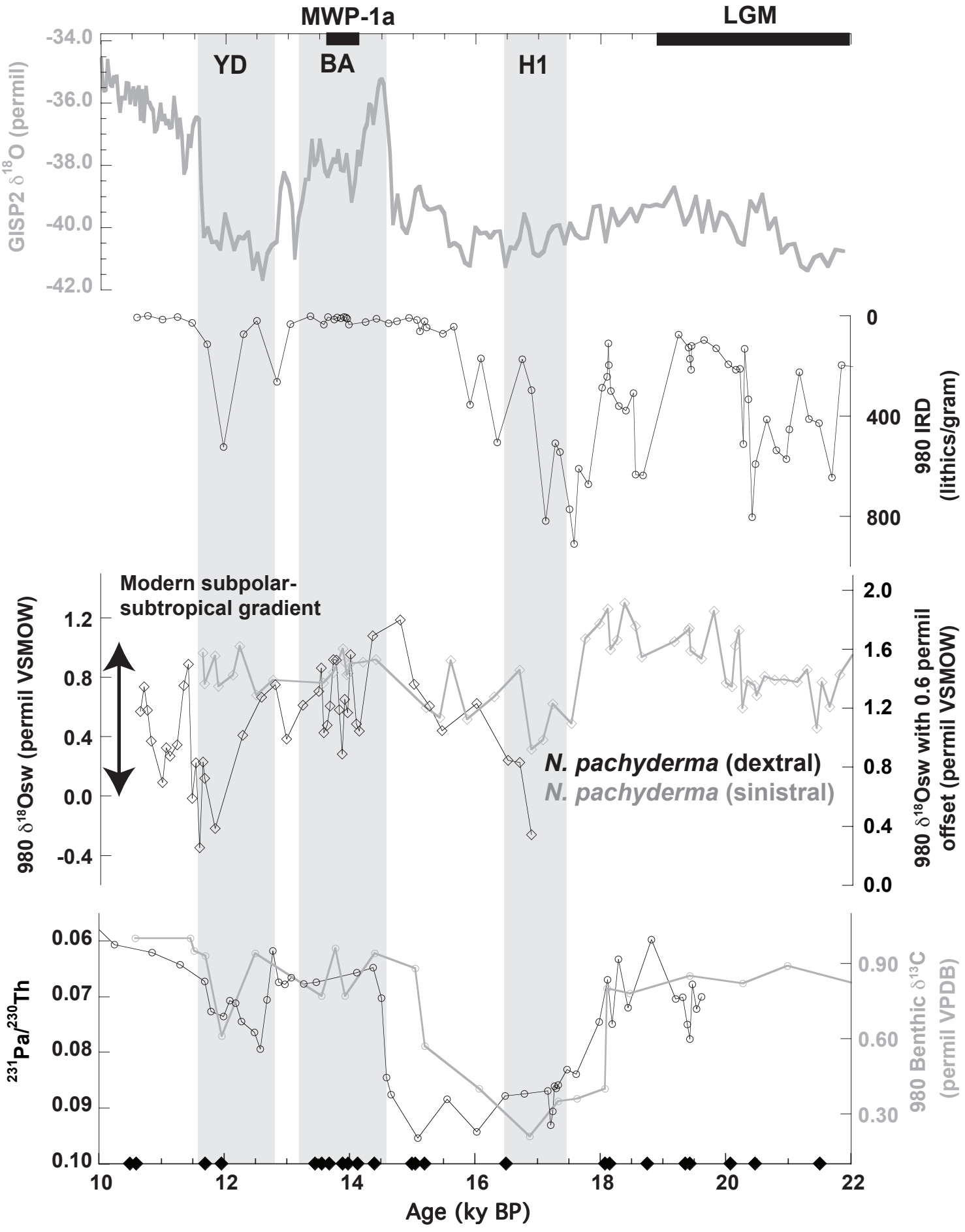
MWP-1a
LGM
YD
BA
H1
GISP2 δ18O (permil)
-34.0
-36.0
-38.0
-40.0
-42.0
980 IRD (lithics/gram)
0
400
800
Modern subpolar-subtropical gradient
980 δ18Osw (permil VSMOW)
1.2
0.8
0.4
0.0
-0.4
N. pachyderma (dextral)
N. pachyderma (sinistral)
980 δ18Osw with 0.6 permil offset (permil VSMOW)
2.0
1.6
1.2
0.8
0.4
0.0
231Pa/230Th
0.06
0.07
0.08
0.09
0.10
980 Benthic δ13C (permil VPDB)
0.90
0.60
0.30
10
12
14
16
18
20
22
Age (ky BP)

Figure 3

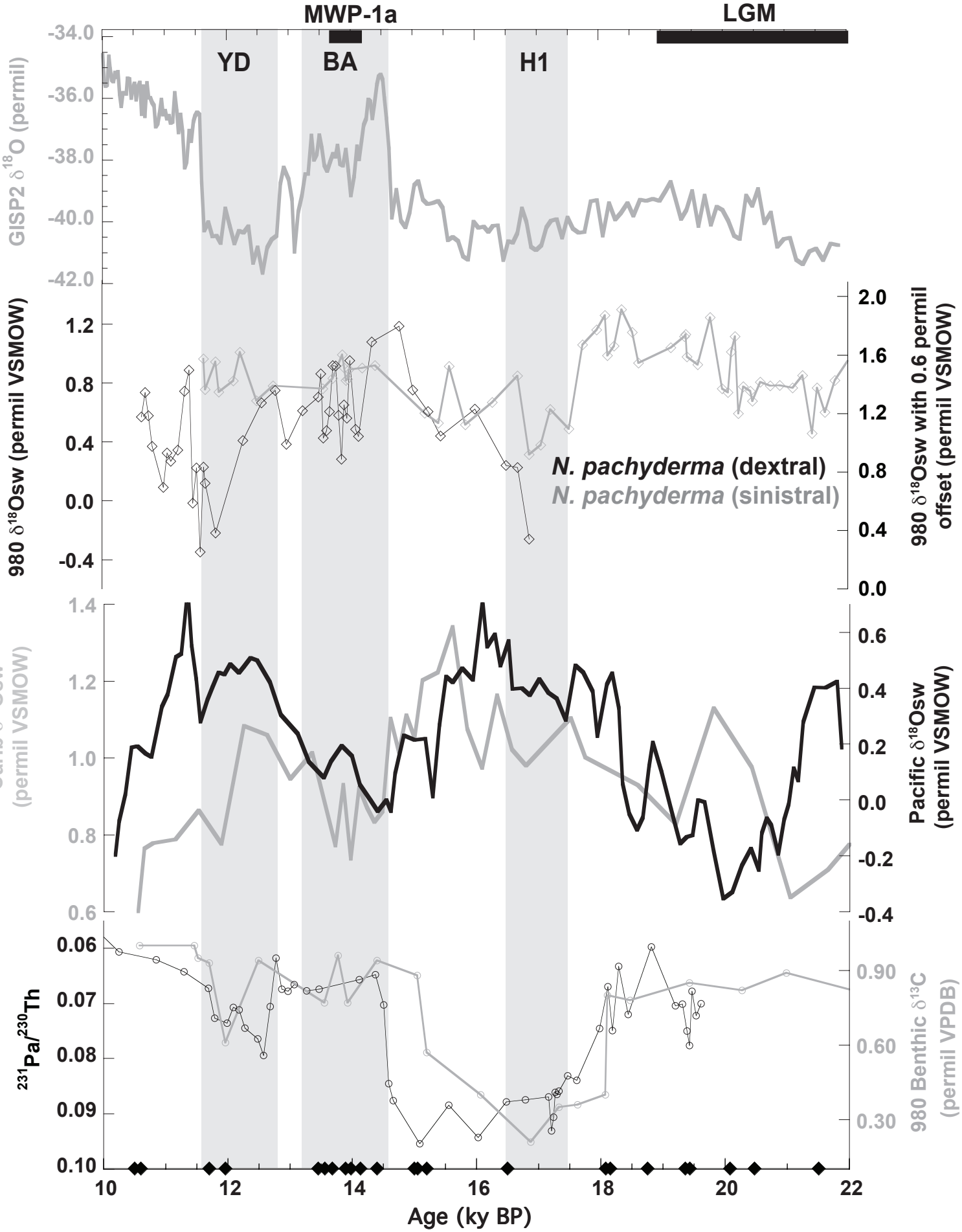
MWP-1a
LGM
YD
BA
H1
GISP2 δ18O (permil)
-34.0
-36.0
-38.0
-40.0
-42.0
980 δ18Osw (permil VSMOW)
1.2
0.8
0.4
0.0
-0.4
980 δ18Osw with 0.6 permil offset (permil VSMOW)
2.0
1.6
1.2
0.8
0.4
0.0
N. pachyderma (dextral)
N. pachyderma (sinistral)
Carib δ18Osw (permil VSMOW)
1.4
1.2
1.0
0.8
0.6
Pacific δ18Osw (permil VSMOW)
0.6
0.4
0.2
0.0
-0.2
-0.4
231Pa/230Th
0.06
0.07
0.08
0.09
0.10
980 Benthic δ13C (permil VPDB)
0.90
0.60
0.30
10
12
14
16
18
20
22
Age (ky BP)

Figure 4

Table 1

ODP 980 Depth (mcd)	Species	^{14}C Age (Yrs BP)	^{14}C Error	Calendar Age (Yrs BP)
0.005	*G. bulloides*	1060	25	636*
0.010	*N. pachyderma (dex)*	1190	35	720*
0.360	*N. pachyderma (dex)*	1710	55	1270*
0.660	*N. pachyderma (dex)*	2910	35	2705*
0.745	*G. bulloides*	3290	35	3140*
0.860	*N. pachyderma (dex)*	3670	40	3575*
1.045	*G. bulloides*	4490	25	4700*
1.160	*G. bulloides*	4880	50	5225*
1.360	*N. pachyderma (dex)*	6240	65	6675*
1.615	*G. bulloides*	7230	70	7680*
1.710	*N. pachyderma (dex)*	7580	50	8010*
1.960	*G. bulloides*	8830	45	9490*
2.310	*N. pachyderma (dex)*	9620	50	10500*
2.495	*G. bulloides*	9780	70	10600*
2.960	*G. bulloides*	10900	55	11700*
3.010	*N. pachyderma (sin)*	11050	50	11960
3.160	*N. pachyderma (sin)*	12050	75	13560
3.160	*N. pachyderma (dex)*	12100	60	13450
3.315	*N. pachyderma (sin)*	12200	55	13890
3.315	*N. pachyderma (dex)*	12450	60	13680
3.410	*N. pachyderma (sin)*	12550	50	13980
3.460	*N. pachyderma (sin)*	12800	70	14400
3.560	*N. pachyderma (sin)*	13100	55	15050
3.560	*N. pachyderma (dex)*	12700	90	14130
3.660	*N. pachyderma (sin)*	13250	55	15200
3.660	*N. pachyderma (dex)*	13050	100	15000
3.810	N. pachyderma (sin)	15300	80	16500
4.020	N. pachyderma (sin)	15350	80	18080
4.120	N. pachyderma (sin)	15450	55	18150
4.275	N. pachyderma (sin)	16000	75	18750
4.320	N. pachyderma (sin)	16450	75	19360
4.420	N. pachyderma (sin)	16650	95	19430
4.520	N. pachyderma (sin)	17200	85	20080
4.720	N. pachyderma (sin)	17750	80	20470
4.920	N. pachyderma (sin)	18500	65	21510

*****Recalibrated ^{14}C dates from Oppo et al. (2003)